Synthesis and properties of Graphene and Graphene/carbon nanotube reinforced soft magnetic FeCo alloy composite by Spark Plasma Sintering

Amar J Albaaji[1*], Elinor G Castle[2,3], Mike J Reece[2,3], Jeremy P Hall[1], Sam L Evans[4]
1-Wolfson Centre for Magnetics, Cardiff School of Engineering, Cardiff University, UK
2-School of Engineering and Materials Science, Queen Mary University of London, UK
3-Nanoforce Technology Ltd., London, UK
4-Institute of Mechanical and Manufacturing Engineering, Cardiff School of Engineering, Cardiff University, UK

Abstract

The effect of the addition of graphene nanoplatelets (GNP) and graphene nanoplatelet/carbon nanotube (GNT) mixtures on the mechanical and magnetic properties of spark plasma sintered (SPS) soft magnetic FeCo alloys was studied. Three different volume fractions (0.5, 1& 2 vol.%) of GNPs and GNTs were investigated. Ball milling was used to disperse the GNPs in monolithic FeCo powder; while magnetic stirring and ultrasonic agitation were used to prepare hybrid GNT prior to ball milling. The highest saturation induction (B_{sat}) of 2.39 T was observed in the 1 vol. % GNP composite. An increase in the volume fraction of the ordered nano crystalline structure was found to reduce the coercivity (*Hc*) of the composites. The addition of CNTs to the GNP composite prevented grain growth, leading to grain refinement. An 18% increase in hardness was observed in the 1 vol. % GNP composite as compared to the as received FeCo alloy. A reduction in tensile strength was observed in all of the composite materials, except for the 0.5 vol.% GNT composite, for which a value of 643 MPa was observed. Raman spectroscopy indicated a reduction in the defect density of the GNPs after adding CNTs.

1. Introduction

Graphene is a material composed of sp2 carbon atoms arranged in a two-dimensional honeycomb structure; and is the strongest material ever recorded [1]. Graphene sheets stack on top of one another, leading to weak van der Waals forces in the c-axis with an approximate separation distance of 3.4 Å. Graphene nanoplatelets (GNPs) typically consist of a ~ 100 nm thick stack of graphene sheets [2, 3]. Due to its unique electrical, thermal and mechanical properties [4, 5], graphene has the potential to significantly improve the properties of materials through its addition as a second phase.

Intermetallic compounds generally exhibit a very low level of ductility at room temperature. Due to the formation of the ordered B2 state, near equiatomic FeCo alloys exhibit very good magnetic properties, yet are extremely brittle at room temperature. Modern power generation systems demand new materials with both good magnetic and mechanical properties. The magnetic properties of FeCo alloys satisfy this requirement, however the mechanical properties of FeCo alloy must be improved in order to meet this need. An

improvement in the ductility of the FeCo alloy has been achieved through grain refinement, reducing the degree of ordering and addition of the alloying element vanadium [6]. Kawahara [7] tested the effect of combined cold working and heat treatment plus the addition of different alloying elements on the magnetic and mechanical properties of FeCo alloys. He reported that the magnetic and mechanical properties are effectively improved by the addition of C, V, Cr, Ni, Nb, Mo, Ta and W. A model for the improvement of ductility in FeCo alloys has been suggested by adding carbon [8]. This addition causes a change in formation and distribution of disorder in the base alloy. A concentrated disordered region could be formed around precipitates, leading to an improvement in ductility. As the order-disorder transformation affects both the mechanical and magnetic properties, an understanding of this transformation during the development of the FeCo alloy is necessary. The ordered phase in the FeCo alloy can only be detected by X-ray diffraction with a Co $K\alpha$ radiant [9, 10].

The use of composite reinforcements to improve the mechanical properties of FeCo was a strategy pioneered by Yu et al. [11]; who, electrodeposited soft magnetic alloys onto *W* fibres. An improvement in mechanical properties was achieved; however, non-soft magnetic behaviour in the as deposited composite was observed due to the stresses introduced by the fabrication process. Powder metallurgy followed by ball milling is considered to be the best route to manufacture extremely brittle FeCo alloy components, since there is more flexibility in the final dimensions and shape and a high mechanical strength can be achieved with little effect on the magnetic properties [12]. A major determining factor in the mechanical performance of material fabricated by a powder metallurgy route is the density. Almost all properties, including strength, ductility and magnetic performance, are improved with increasing density [13].

The spark plasma sintering (SPS) process has been used extensively in the last decade to densify a wide variety of powdered materials. The application of high pressure and pulsed DC current to the electrically conductive dies leads to rapid heating and sintering. As such, the technique makes it possible to achieve high densities, close to theoretical density, without prior compaction or binder addition. The rapid nature of the technique enables the characteristics of the starting powder to be transferred to the final sintered part; such as a fine grain size, metastable phase or composition or inclusion of volatile elements. The application of a current during processing has been shown to ‘clean’ the powder particles of surface oxides [14, 15]. Many studies have employed SPS to sinter CNT composites and nanopowders with the aim of restricting grain growth [2, 16]. Mani et al. obtained 99% theoretical density and a saturation induction (B_{sat}) of 2.33 T in a Fe-50% Co alloy prepared by SPS at 900°C for 2-5 min under a pressure of 80 MPa [17]. Recently, a Ni-P electroless coated CNT-reinforced Fe-50Co composite was fabricated by ball milling and SPS processing; an improvement in ductility and strength was observed, at the expense of the magnetic properties [18]. The phase transformation of metal magnetic alloys during processing effects the processing parameters of the SPS furnace, making it is possible to calibrate temperature [19].

While extensive research has been published on polymer-graphene composites [1] and to a lesser extent on ceramic-graphene composites [20], to the best of our knowledge there

are very limited publications on metal graphene composites; especially FeCo alloys. Issues involving the formation a stable dispersion of graphene nanoplatelets (GNPs) are rather complicated as compared to carbon nanotube (CNTs) since GNPs tend to agglomerate and restack on one another during dispersion and drying.

Kim et al. [21] used graphene oxide as a dispersion agent for both multiwall and single wall carbon nanotubes in water. The authors demonstrate that graphene oxide is able to strongly interact with the surface of CNTs throughout π-π attractions due to many π-conjugated on the surface of graphene oxide. This inspired researchers to insert 1-D reinforcement CNTs amongst GNP sheets, which could potentially prevent restacking and agglomeration. Wimalasiri et al. [22] have used single walled carbon nanotubes (SWCNTs) to prevent restacking between graphene sheets when they fabricated electrodes from carbon nanotube and graphene composite. Increasing the space between graphene using CNTs improves the transport of electrolyte ions within the electrode. This strategy has been previously tested in ceramic [23, 24], polymer [25] and light weight metal alloy [26] based systems. Excellent mechanical properties due to improved dispersions were achieved. So far, there has been no systematic study into the use of CNTs to improve the dispersion of GNPs in soft magnetic FeCo alloys.

This article outlines the results from a study into the effects of GNP and CNT additions on the structural, magnetic and mechanical properties of Fe-Co composites fabricated by ball milling and SPS.

2. Material and Method

2.1. Starting materials

Gas atomised FeCo alloy powder was supplied by Sandvik Osprey Powder Group. The mean size of powder, measured by Malvern Mastersizer 3000 with laser scattering, is 23.4 μm. Multi-walled carbon nanotubes (MWCNT) and graphene nanoplatelets (GNP) were provided from Haydale Ltd. They are functionalized by plasma treatment to incorporate covalently bonded oxide group on their surfaces.

2.2. Powder mixing

GNP was dispersed in FeCo powder by using Spectromill ball pestle impact grinder in air atmosphere (Chemplex Industries Inc., Model 1100) with steel ball pestles with a ball to powder ratio (BPR) of ~1:1 for 1h. Three different volume fractions (0.5, 1 & 2 vol. %) of GNP were dispersed in 20 g of FeCo powders. The mixture of CNT and GNP referred to as GNT, was also used as reinforcement for soft magnetic FeCo alloy at same volume fraction. The mixing ratio of CNT: GNP was 1:10. The theoretical densities used to calculate of the volume fractions using a rule of mixture are 1.4 g/ccm, 2.2 g/ccm and 8.174 g/ccm for CNT, GNP and FeCo powder respectively. GNT was magnetically stirred in 100 ml of ethanol for 0.5 h, followed by ultrasonication for 0.5 h. 20 g of FeCo powder was mixed with GNT to form composite slurry. The composite mixture was tip sonicated for 1 h in 150 ml ethanol.

Drying was performed by heating at 80 ˚C on hot plate overnight. After drying, the powder was ball milled using the same conditions described for the GNP dispersions.

2.3. SPS fabrication

20 g of FeCo alloy powders and composite powder mixtures were consolidated in a graphite die lined with graphite foil using a spark plasma sintering furnace (HPD 25/1 FCT, Germany) at Queen Mary University of London. All of the samples were heated to the sintering temperature at a constant rate of 50˚C min^{-1} under a vacuum of 1.5 Pa. The initial 7 MPa pressure was applied to 400˚C; followed by an increase to 80 MPa pressure and simultaneous heating to 900 °C for a 3 minute soak at this temperature [17]. After rapid cooling in contact with the water cooled pistons of the spark plasma sintering furnace, the samples were manually extracted from the die using a hydraulic press.

2.4. Characterisation

In order to measure the density of the sintered materials, the graphite layer was removed from surface of sintered materials by grinding with Emery paper. The density was measured using Archimedes' immersion method in water.

To evaluate the structure of raw nanomaterials, a high resolution Transmission Electron Microscope (TEM) (JEM-2100 LaB6) was used to evaluate the as received GNPs and CNTs.

For optical microscopy analysis, cross sections of the sintered materials were ground and polished with different grade abrasive discs followed by etching using 10 % Nital for 30 sec. Scanning Electron Microscopy (SEM) (Oxford instruments) was used to analyse the fracture surfaces of the tensile samples.

The crystallographic phases and ordering state present in the as received and composite materials were examined using X-Ray Diffraction (XRD) (Philips PW 3830 Automated Powder Diffraction) supplied with a Co target X-ray tube. The scans were performed between 10 and 110 $^{\circ}2\theta$ at a scan speed of 8 x 10^{-3} $^{\circ}2\theta\ sec^{-1}$ at operation conditions of 35 kV and 40 mA. A slow scan was performed in the expected $^{\circ}2\theta$ range of the ordered phase at a scan speed of 25 x 10^{-5} $^{\circ}2\theta\ sec^{-1}$ and operating conditions of 42 kV and 40 mA.

Raman spectroscopy was performed on the GNP and CNT powders and on tensile samples of composites of different volume fractions (using Renishaw in Via Raman microscope). The excitation wavelength was maintained at 514 nm for all samples with a power of 25 mW and spot size of 5 µm. The Raman spectra scans between 1000 and 3200 cm^{-1} were obtained after 15 accumulations.

2.5. Mechanical and magnetic properties

Tensile tests were performed on 3 samples cut from the 30 mm diameter monolithic FeCo alloy and composites discs by electron discharge machining (EDM). The cut samples were ground with silicon carbide to remove any crack initiation sites produced by cutting. Tensile properties were evaluated using a Shimadzu testing machine with a cross head speed

of 2 mm/min. The tensile sample dimensions in mm were 11 x 3 x 1.25 [27]. Hardness measurements for both the matrix alloy and composite were performed at five different locations using a Vickers hardness tester using 30 g load for 4 sec.

In order to evaluate the magnetic properties, samples with a rectangular cross section 24 mm x 5 mm were cut from the 30 mm diameter sintered discs using an EDM cutting machine. Samples were ground using Emery paper to remove the scratches produced during cutting. An automatic universal measurement system was used to evaluate the quasi DC magnetic response for samples by changing the magnetic field up to 25 kA m^{-1} [28].

3. Results and discussion

3.1. TEM analysis of nano powder

The graphene nanoplatelets and carbon nanotube morphologies are shown in (Fig.1). A wrinkled morphology is observed for the GNPs, which may produce porosity in the composites. A variety of sizes were observed, and very small sheets were observed to be stacked on larger sheets. The thickness of the GNP sheets ranges from ~ 4 to 42 nm. The width of the sheets ranges from ~ 27 to 223 nm, while the length varies from ~ 85 to 487 nm. Most of CNTs are tangled together, which impedes their dispersion. The measured dimensions of the CNTs exhibit a mean outer diameter of around 10.45 nm, while the inner diameter is around ~ 4 nm (corresponding, to ~ 10 concentric shells of carbon sheets).

3.2. Optical microstructure

The optical micrographs of the monolithic FeCo alloy and composite materials are shown in (Fig.2). The as received monolithic FeCo alloy consists of grains of uniform size, as shown in (Fig.2. (a)). The sintered samples prepared with powders that had been ball milled contained elongated grains , as shown in (Fig.2. (b)).

The microstructure of the GNP composites was inhomogeneous (Fig. 2. (c)) with excessively growth grains surrounded by small grains. Adding a small amount of CNTs (1:10) significantly change the microstructure. The homogenous microstructure observed may result from the uniform dispersion of the nanophases and the prevention of the restacking of the nanophases. Fig. 2. (d) shows the refined microstructure, which is occurred due to the addition CNTs to GNPs as compared to the GNP composite (Fig. 2. (c)).

An increase in the volume fraction of reinforcement leads to the introduction of agglomerates, which results in increased porosity. The preferential etching of agglomerated GNPs by Nital leads to strings of pits which decorate the grain boundaries, as shown in the back scattered image in (Fig. 3. (b)) as compared to monolithic FeCo alloy image in (Fig. 3. (a)). The porosity formed around agglomerated GNPs lead to reduce interfacial bonding, reducing the efficiency of load transfer to the reinforcement and a site for crack initiation.

Impurity elements such as (O, N, H_2) may segregate at grain boundaries, grain boundaries were investigated using EDX spectra. The spectra were taken from the grain

boundaries of sintered 1 vol. % GNP and FeCo alloy did not shown any difference in chemical composition between materials.

3.3. Densification of sintered FeCo composites

The relative density of the spark plasma sintered FeCo-GNP and FeCo-GNT compacts are shown in (Fig.4). Almost full densification was achieved for the as received FeCo compact, with a relative density higher than 99%. In comparison, the final density of the FeCo alloy after 1 h ball milling was reduced to 98%. The addition of reinforcements increased the final density in comparison to the ball milled FeCo alloy, yet decreased overall with increasing volume fraction of reinforcement. The density of the GNT composites was lower as compared to the GNP composites, which might be attributed to the presence of carbon nanotubes in the GNT composites. The 2D morphology of the GNPs leads to a higher surface area as compared to the 1D carbon nanotubes. An increase in the contact area between the GNPs and the matrix alloy leads to a higher density; while, CNTs inserted between the GNPs may introduce porosity between the sheets and reduce the density. However, at the higher volume fraction the agglomeration of the GNPs at the grain boundaries was observed, leading to lower densification.

The effects of ball milling and the addition of nano reinforcements on the sintering mechanisms were examined by plotting the change in average piston speed, average force and temperature against time (Fig.5). The average piston speed data shows difference between the as received FeCo alloy compared to the other sintered materials.

The peak in the average piston speed of the as received FeCo alloy was achieved at 700 sec, while the maximum in average piston speed for the other sintered materials was achieved at 600 sec. Fine particle size and imperfections such as dislocations, which are introduced during ball milling reduced the densification time of 1h ball mill FeCo powder as compared to as a received FeCo powder. Increasing the surface area due to refining reduces diffusion paths and improves densification. However, the density was lower in the 1 h ball milled FeCo compact as compared to as received FeCo compact which may be due to oxidation during the milling in air. Small differences in the shrinkage curves are observed between the composites. This could be explained by the difference in packing of the GNP composites compared to the GNT composites, which occurs as result of changing morphology from the two dimensions of GNP to the three dimensions of the CNT-GNP mixture.

3.4. Analysis X-ray diffraction results of raw materials and FeCo composites

XRD patterns of the sintered FeCo alloy and its composites are presented in (Fig.6). In spite of the slow X-ray scan rate used for all of the FeCo alloy composites, the distinctive 2θ =26.5° peak of the GNPs was not observed due to its relatively low volume fractions, which are beyond the sensitivity of the XRD technique. To clarify any shift in peaks position, the figure was enlarged, as shown in the insert (Fig.6). The fundamental peaks were shifted to lower angles in the composite materials as compared to the as received FeCo alloy. This is due to the stresses introduced during ball milling. A broadening of the XRD peaks was also observed in the composite materials, due to microstructure refinement following ball milling.

The volume fraction of the ordered state has an effect on both the magnetic and mechanical properties of FeCo alloys. A very slow scan rate and high intensity XRD (Co Kα) was employed in order to investigate the (100) super-lattice line reflection of the sintered FeCo alloy, 1 h ball milled FeCo alloy, GNT and GNP composites as shown in (Fig. 7). The long range ordering fraction in FeCo alloy has been shown to reduce following ball mill [29]. With a 1 vol. % GNP dispersion in the FeCo alloy an increased volume fraction of ordering was observed. However, the introduction of 2 vol. % GNP did not make any significant difference to the degree of ordering and crystallite size. The intensity of the super lattice reflection was found to be higher in the GNP composites as compared to the GNT composites; indicating a greater volume fraction of ordering in the GNP composite. This is confirmed by the shift of the peak to lower angles in the GNP composites due to the strains induced by the more significant ordering reaction as compared to the GNT composites. Clegg and Buckley [30] reported that the change in lattice parameter between the disordered and ordered phases is about 0.2%; varying from 0.28550 to 0.28570 nm. The anti-phase domain sizes were estimated from the super lattice line in (Fig.7) using the Scherrer equation. A significant reduction in the anti-phase domain sizes was observed in the 1 vol.% GNT composite, which reflects the role of carbon nanotubes in refining the crystallite structure or due to improved dispersion, while GNP additions did not influence the nanostructure.

3.5. Magnetic properties

The upper half of the magnetic hysteresis curves of the as received FeCo monolithic alloy and its composites are shown in (Fig.8). A summary of the magnetic induction ($B_{sat.}$), coercivity (H_c) and remanence (B_r) of the materials is shown in (Fig.9). An increase in saturation induction and reduction in coercivity is observed in the GNP composites compared to as received FeCo alloy, for reinforcement additions up to 1 vol. %. In general, a higher remanence is observed in the GNT composites as compared to the GNP composites (Fig. 9 inset). In order to separate the effects of ball milling from the effect of reinforcement on the magnetic properties, the 1 h ball milled FeCo compact was also investigated. The saturation induction of 1 h ball milled FeCo compact was reduced from (2.30 T) to (2.23 T), while exhibiting a decline in coercivity from (836 A/m) to (763 A/m).

It was shown in the previous section that the density after ball milling under air atmosphere dropped, which can account for the reduced in saturation induction due to oxide formation [29]. The 1 vol. % of GNPs composite exhibited a higher saturation induction value of (2.39 T) than the 1 h ball mill FeCo alloy (2.23 T) due to the increase in density produced by the addition GNPs to the ball milled FeCo alloy as confirmed in (Fig. 4). However, with addition of 1 vol. % of GNTs the saturation induction dropped to (2.12 T). The increased space between GNPs due to inserting CNTs leads to drop in density due to porosity (Fig. 4). Further, the increased saturation in GNP composite can also be explained by the ferromagnetic behaviour of graphene and improved electrical conductivity of this composite [31, 32], which could affect the densification processes during SPS and subsequent magnetic properties. The 2D form of the GNPs exhibits open edges, in contrast to the inserted CNTs which have closed π-electron systems. The nonbonding state also creates nanomagnetic properties at edges [33]. While, the inserted CNTs will influence magnetic

properties primarily due to the introduction of porosity and due to the presence of any residual metallic catalysts on their surface.

The coercivity is very sensitive to changes in microstructure. The coercivity after ball milling under air atmosphere dropped, which may have been caused by the formation of nanocrystalline structure. The slow scan rates XRD (Co Kα) patterns (Fig. 7) revealed a (100) super lattice reflection with crystallite dimensions reduced to nanoscale. It has been shown [33, 34] that at this scale the trend in coercivity would follow that of the average magneto-crystalline anisotropy when the crystallite size becomes less than the ferromagnetic exchange length, leading to a drop in coercivity. The composites with GNT displayed a higher coercivity than the GNP composites, which is due to the more refined grain size (Fig. 2. (d)) of GNT composite as a result of better dispersion. The restacking of GNPs increased at higher volume fraction composites, leading to an increase of the particle size of the GNPs to micron size, which decreases the effectiveness of GNPs to reduce grain growth.

3.6. Mechanical properties

The tensile strength and the mechanical hardness of the as a received monolithic FeCo alloy (represented as 0 vol. % reinforcement) and the composites with different volume fraction of GNPs and GNTs are summarised in (Fig.10.) and (Fig.11.) respectively. The 1 h ball milled FeCo compact was also examined and compared to alloy prepared with unmilled powder exhibited a decrease in ultimate tensile strength from (673 ±17.43 MPa) to (643 ±40 MPa), failure strain was also dropped from (2.9 ±0.70 %) to (2.4 %), while the hardness increased from (326.5 ±18 VHN) to (355.7 ±5 VHN).

Hard oxides formed during ball milling lead to an increase in hardness, yet hindered densification process and hence lower the tensile strength and failure strain. The addition of GNPs to the FeCo alloy led to a decrease in tensile strength. This was possibly due to the restacking of GNP sheets as shown in (Fig. 13. c), which cause easily slip in GNPs with respect to one another and separate under stresses. Strength arising from nano-reinforcement mechanisms will deteriorate once the GNPs become agglomerated into micro-sized clusters, reducing the tensile strength by acting as stress concentrators. An improvement in tensile strength was subsequently observed in the hybrid GNT composite, where the addition of CNTs prevets agglomeration of the GNPs

A marked increase in hardness to 385.3 ±35 VHN was observed in the FeCo-1 vol.% GNP composite, as shown in (Fig. 10.). This represents an 18% increase in hardness in comparison to the as received FeCo alloy. The highest density value among the composite materials was achieved for the 1 vol. % GNP composite, leading to increase in hardness. The hardness decreased for the 2 vol. % GNP composite, because of the decrease in density produced by agglomeration of GNPs.

Fig. (11) shows failure strains with volume fraction of reinforcement, the composite material exhibit decrease in failure strain especially at higher loading as compared to as received FeCo alloy, confirming increased brittleness in FeCo alloy from agglomeration.

Fig. 12 shows a comparison between the fracture surfaces of monolithic FeCo alloy, 1 vol. % GNP composite and 1 vol. % GNT composite. Mixed mode of intergranular and transgranular fracture predominate in all of the sintered materials, indicating that the inherent weakness of grain boundaries cannot be avoided by the nanophase additions.

Evidence of toughening mechanisms, such as crack deflection and platelet pull out are observed in (Fig.13 a, c). A large GNP can be seen to warp around a grain. It is expected that the flexibility of GNPs allows them to bend around and become embedded between the grains during sintering. The large surface area of GNPs increases the contact area with the matrix, leading to an increased interfacial force, requiring more energy to pull out the GNP sheets as compared to the CNTs. However, overlapping between GNPs decreases the interface bonding efficiency. It is observed that thin GNP sheets are effective at inhabiting crack propagation as compared to thick overlapped GNP sheets, which are easily sheared and form pores, degrading the mechanical and physical properties. The CNTs are embedded between the GNPs as observed in (Fig.13 d); pull-out of the CNTs occurred during fracture. The high aspect ratio of the CNTs allows them to bridge the fracture surface, as shown in (Fig.13 b).

3.7. Raman spectroscopy

Graphene is routinely characterised using Raman spectroscopy. In a typical Raman spectrum of single layer graphene the main peaks are seen at 1583 cm^{-1} (commonly referred to as G), D peak at 1350 cm^{-1} and the shoulder D' at around 1620 cm^{-1}. In addition to this: the overtone peak, 2D or G', appears at 2680 cm^{-1}; the D+G peak appears at around 2950 cm^{-1}, the 2D' peak appears at 3245cm^{-1}; and finally the 2D+G peak occurs at 4290 cm^{-1}[36]. The ratio I_D/I_G is typically used to measure the disorder and defect density in graphene, while the strain in graphite can be observed as a shifting and splitting of the Raman modes [37]. A comparison of Raman spectra of the CNTs and GNPs is shown in Fig.14. Raman spectra of the as received GNT, FeCo alloy and the FeCo alloy-GNP and GNT composites are shown in Fig.15. The FeCo alloy does not produce any Raman signals. The structure of GNP was retained after all of the fabrication processes as evidenced from the shape of the single-peak shape of the 2D band in the Raman spectrum; indicating the presence of the graphene morphology as opposed to the graphite morphology, which would give rise to a split-peak [38].

Table 1 lists the peak intensity ratio *($R=I_D/I_G$)*, the position of the G and 2D peak positions. The GNPs were observed to be of higher quality than the CNTs, as evidenced from the lower *R* ratio of the GNPs (1.00) compared to CNTs (1.11). An increase in *R* ratio was observed for all of the composites. This was particularly notable for the GNP composites as compared to the as received GNPs. This may have resulted from an interfacial reaction of the matrix with the side wall of the GNPs, or could have induced by ball milling. However, this ratio decreased in the GNT composites as compared to the GNP composites, suggesting that the addition of CNT to GNP in ethanol may help to maintain the structure of the GNP. High quality for vacuum during sintering process is crucial to preservation carbon nanostructure in

sintered composites materials [39]. The oxidation for reinforcement was reduced due to using a good vacuum (1.5 Pa), helping to improve the quality of carbon nanostructure.

Strains are induced in the GNPs by the fabrication processes and by mechanical testing of the composite material. Such strains will lead to alterations in the interatomic distance of the graphene. The G band peak position is very sensitive to strain in the graphene structure. Hence the shift in wave number will change according to alteration in the vibration frequency of the G band due to strain [37]. Up shifting was observed in the peak position of the G-band (ω_G) peak for the composites in comparison to the as received GNP. A shift of between 8.6 cm^{-1} to 22.8cm^{-1} is observed in the GNP composites as compared to the as received GNP; and a 10.6 cm^{-1} to 13.6 cm^{-1} shift is observed for the GNT composites. This indicates that significant strains have been induced in the GNPs in the aforementioned composites.

Up shifting is also observed in the 2D peak. Since the 2D band peak is very sensitive to the number of layers in graphene, a change in position, width and shape could occur in the 2D peak with an increasing number of layers [38]. The shifting was reduced in 1 and 2 vol. % GNT composite indicating that less overlapping had occurred between the GNP sheets as a result of the addition CNTs.

4. Conclusions

Composites containing 1 vol. % GNP displayed the highest saturation induction (2.39 T) and the lowest coercivity (583 A/m); while the remenance values were higher in the GNT composites than GNP composites for the same loading. The mechanical properties reveal a maximum increase in hardness of 18% for the 1 vol. % GNP composite. The highest tensile strength observed in the composite materials occurred in the 0.5 vol. % GNT composite. Long range ordering was promoted in the FeCo alloy by the addition of GNPs. Adding CNTs to the GNPs in FeCo leads to a more uniform and refined structure. However, porosity was induced leading to a decrease in the density of the GNT composites. Raman spectra show that the quality of the GNPs was improved by adding CNTs, which reduce the amount of overlapping of the GNP sheets.

References

[1] Kim, H., Abdala, A. a. & MacOsko, C.W., 2010. Graphene/polymer nanocomposites. *Macromolecules*, 43(16), pp.6515–6530.

[2] Tjong, S.C., 2013. Recent progress in the development and properties of novel metal matrix nanocomposites reinforced with carbon nanotubes and graphene nanosheets. *Materials Science and Engineering R: Reports*, 74(10), pp.281–350.

[3] Lian-Yi Chen, Hiromi Konishi, Axel Fehrenbacher, Chao Ma, Jia-Quan Xu, B. & Hongseok Choi, Hui-Fang Xu, F.E.P. and X.-C.L., 2012. Novel nanoprocessing route for bulk graphene nanoplatelets reinforced metal matrix nanocomposites. *Scripta Materialia*, 67(1), pp.29–32.

[4] Xiao Huang, Xiaoying Qi, F.B. and H.Z., 2012. Graphene-based composites. *Chemical Society Reviews*, 41(2), pp.666–686.

[5] Zhong-Shuai Wua, Guangmin Zhoua, Li-Chang Yina, W.R. & Feng Lia, H.M.C., 2012. Graphene/metal oxide composite electrode materials for energy storage. *Nano Energy*, 1(1), pp.107–131.

[6] Mitsuhiro Matsuda, Kozo Yamashita, R.S. & Kenji Akamine, K.T. and M.N., 2013. Development of Ductile B2-Type FeCo Based Alloys. *Materials Transactions*, 130464(10), pp.1–6.

[7] Kawahara, K. & Uehara, M., 1984. A possibility for developing high strength soft magnetic materials in FeCo-X alloys. *Journal of Materials Science*, 19(8), pp.2575–2581.

[8] Kawahara, K., 1983. Effect of carbon on mechanical properties in Fe0.5Co0.5 alloys. *Journal of Materials Science*, 18, pp.2047–2055.

[9] G. B. Chon, K. Shinoda, S.S. and B.J., 2010. Order-Disorder Transformation in Fe50Co50 Particles Synthesized by Polyol Process. *Materials Transactions*, 51(4), pp.707–711.

[10] Loureiro, J.M. et al., 2011. Order-disorder phenomena from X-ray diffraction in FeCo alloys annealed and ground at high energy. *Powder Diffraction*, 26(03), pp.267–272.

[11] Yu, R.H., Ren, L., Basu, S., Unruh, K. M., Parvizi-Majidi, A. and John Xiao, Q., 2000. Novel soft magnetic composites fabricated by electrodeposition. *Journal of Applied Physics*, 87(9), pp.5840–5842.

[12] Zafer Turgut, Meiqing Huang, John C. Horwath, and R.T.F., 2008. High strength bulk Fe-Co alloys produced by powder metallurgy. *Journal of Applied Physics*, 103(7), pp.131–134.

[13] Rutz H.G. and Hanejko F.G., 1994. High density processing of high performance ferrous materials. *International conference and exhibition on powder metallurgy and particulate materials*, May 8-11, 1994. TORONTO, CANADA.

[14] Xü, C.Y., Jia, S.S. & Cao, Z.Y., 2005. Synthesis of Al-Mn-Ce alloy by the spark plasma sintering. *Materials Characterization*, 54, pp.394–398.

[15] Groza, J.R.M.G.J.A.S., 2001. Surface effects in field-assisted sintering. J. Mater.Res.,16(1), pp.286–292.

[16] Munir, Z., Anselmi-Tamburini, U. & Ohyanagi, M., 2006. The effect of electric field and pressure on the synthesis and consolidation of materials: A review of the spark plasma sintering method. *Journal of Materials Science*, 41(3), pp.763–777.

[17] Mahesh Kumar Mani, Giuseppe Viola, Mike J Reece, Jeremy P Hall, S.L.E., 2012. Structural and magnetic characterization of spark plasma sintered Fe-50Co alloys. *Mater. Res. Soc. Symp. Proc.*, 1516, pp.201–207.

[18] Mahesh Kumar Mani, Giuseppe Viola, Mike J. Reece, Jeremy P. Hall, S.L.E., 2014. Improvement of interfacial bonding in carbon nanotube reinforced Fe-50Co composites by Ni-P coating: Effect on magnetic and mechanical properties. *Materials Science and Engineering B: Solid-State Materials for Advanced Technology*, 188, pp.94–101.

[19] Mahesh Kumar Mani, GiuseppeViola, JeremyP.Hall, S. & J.Reece, M., 2015. Observation of Curie transition during spark plasma sintering of ferromagnetic materials. *Journal of Magnetism and Magnetic Materials*, 382, pp.202–205.

[20] Porwal H, Grasso S, Reece M. 2013. Review of graphene–ceramic matrix composites. *Adv. Appl. Ceram.*, 112(8), pp.443-454.

[21] Jaemyung Kim, Laura J. Cote, Franklin Kim, Wa Yuan, Kenneth R. Shull, A. & Huang, J., 2010. Graphene Oxide Sheets at Interfaces. *J. AM. CHEM. SOC.*, 132(23), pp.8180–8186.

[22] Yazdani, B., Porwal, H., Xia, Y., Yan, H., Reece,M.J., Zhu, Y., 2015. Role of synthesis method on microstructure and mechanical properties of graphene/carbon nanotube toughened Al2O3 nanocomposites. *Ceramics International*, 41(8), pp.9813–9822.

[23] Yazdani, B., Xia, Y., Ahmad, I., Zhu, Y., 2015. Graphene and carbon nanotube (GNT)-reinforced alumina nanocomposites. *Journal of the European Ceramic Society*, 35(1), pp.179–186.

[24] Pin-Ning Wang, Tsung-Han Hsieh, Chin-Lung Chiang, and M.-Y.S., 2015. Synergetic Effects of Mechanical Properties on Graphene Nanoplatelet and Multiwalled Carbon Nanotube Hybrids Reinforced Epoxy / Carbon Fiber Composites. Journal of Nanomaterials, 2015, pp.1-9.

[25] Muhammad Rashad, Fusheng Pan, Aitao Tang, Muhammad Asif, M.A., 2014. Synergetic effect of graphene nanoplatelets (GNPs) and multi-walled carbon nanotube (MW-CNTs) on mechanical properties of pure magnesium. *Journal of Alloys and Compounds*, 603, pp.111–118.

[26] Wimalasiri, Y. & Zou, L., 2013. Carbon nanotube/graphene composite for enhanced capacitive deionization performance. *Carbon*, 59, pp.464–471.

[27] George E. Dieter. 1986. *Mechanical Metallurgy*. 3th ed. McGraw-Hill.

[28] Anderson, P. 2008. A universal DC characterisation system for hard and soft magnetic materials. *Journal of Magnetism and Magnetic Materials* 320(20), pp. 589-593.

[29] Mahesh Kumar Mani, Giuseppe Viola, Mike J. Reece, Jeremy P. Hall, S.L.E., 2014. Fabrication of carbon nanotube reinforced iron based magnetic alloy composites by spark plasma sintering. *Journal of Alloys and Compounds*, 601, pp.146–153.

[30] Clegg, D.W. & Buckley, R. a., 1973. The Disorder → Order Transformation in Iron–Cobalt-Based Alloys. *Metal Science*, 7(1), pp.48–54.

[31] Yuan, B., Yu, L., Sheng, L., An, K. and Zhao, X., 2012. Comparison of electromagnetic interference shielding properties between single-wall carbon nanotube and graphene sheet/polyaniline composites. *Journal of Physics D: Applied Physics*, 45(23), pp.1–6.

[32] P. K. Sahoo, Bharati Panigrahy, Dan Li, and D. Bahadur, 2013.Magnetic behavior of reduced graphene oxide/metal nanocomposites. *Journal of Applied Physics*, 113, 17B525, pp.1-3.

[33] Enoki, T. & Kobayashi, Y., 2005. Magnetic nanographite: an approach to molecular magnetism. *Journal of Materials Chemistry*, 15(37), p.3999.

[34] Herzer, G., 1990. Grain Size Dependence of Coercivity and Permeability in Nanocrystalline Ferromagnets. *IEEE Transactions on Magnetics*, 26(5), pp.1397–1402.

[35] H Q WU, D M XU, Q WANG, Y Z YAO, Q.Y.W. and G.Q.S., 2008. Effect of heat treatment on structure and magnetic properties of FeCoNi/CNTs nanocomposites. *Bull. Mater. Sci.*, 31(5), pp.801–806.

[36] C. N. R. Rao, A. K. Sood, K. S. Subrahmanyam, and A.G., 2009. Graphene: The New Two-Dimensional Nanomaterial. *Angewandte Chemie International Edition*, 48(42), pp.7752–7777.

[37] Mina Bastwros, Gap-Yong Kim, Can Zhu, Kun Zhang, Shiren Wang, X.T. & Wang, X., 2014. Effect of ball milling on graphene reinforced Al6061 composite fabricated by semi-solid sintering. *Composites Part B: Engineering*, 60, pp.111–118.

[38] A. C. Ferrari, J. C. Meyer, V. Scardaci, C. Casiraghi, M. Lazzeri, F. Mauri, S. Piscanec, D.J. & K. S. Novoselov, S. Roth, and A.K.G., 2006. Raman spectrum of graphene and graphene layers. *Physical Review Letters*, 97(18), pp.1–4.

[39] Inam, F., Yan, H., Reece, M., Peijs, T. 2010.Structural and chemical stability of multiwall carbon nanotubes in sintered ceramic nanocomposite. *Advances in Applied Ceramics*, 109(4), pp. 240-245.

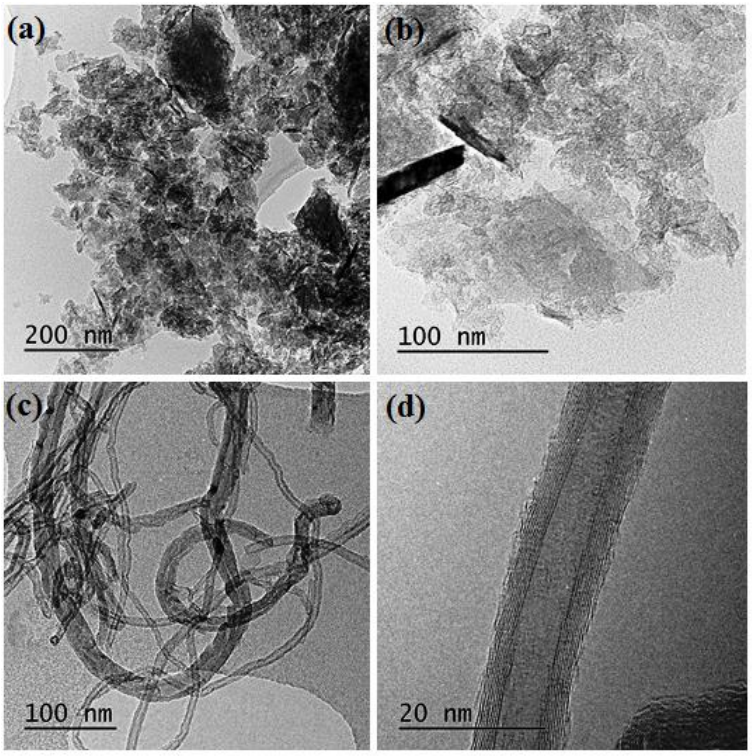

Fig.1. Transmission Electron Microscope (TEM) of; (a, b) GNP and (c, d) CNT.

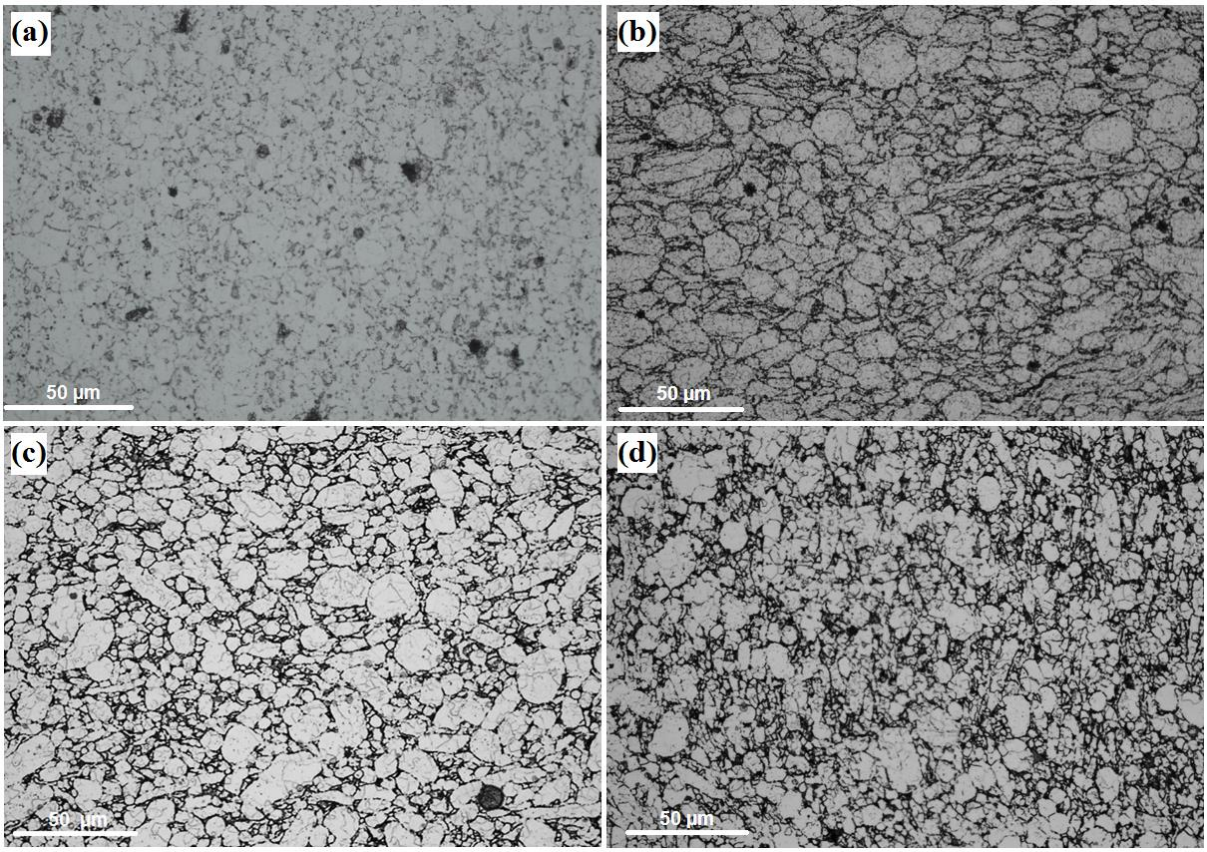

Fig.2. Optical microstructure of: (a) as received FeCo alloy; (b) 1 h ball milling FeCo compact (c) 2 vol.% GNP composite (d) 2 vol.% GNT composite.

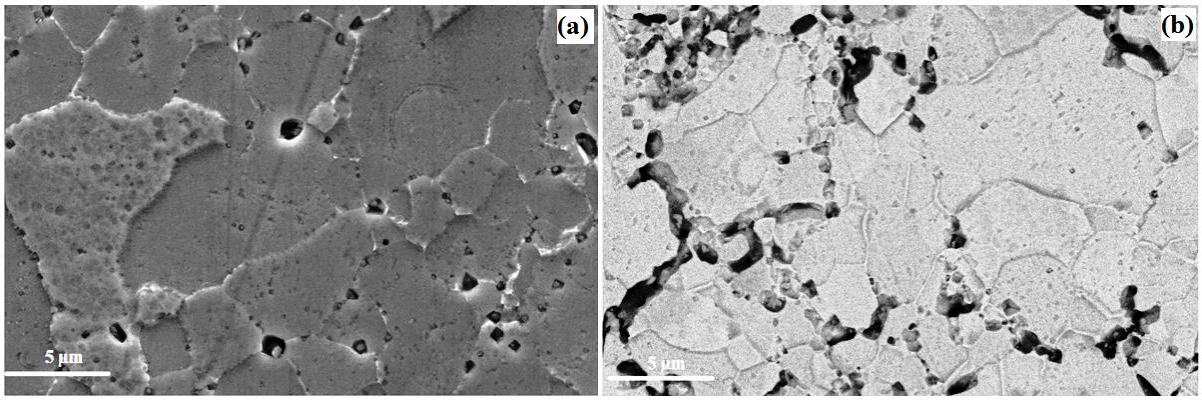

Fig.3. SEM microstructure for (a) FeCo alloy and (b) back scatter of 1 vol. % GNP composite.

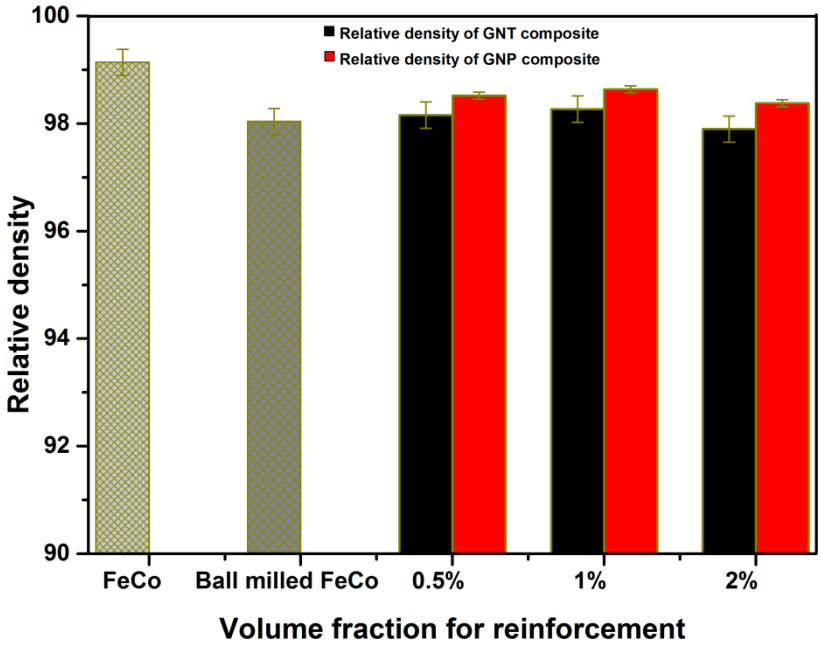

Fig.4. Variation of relative density of SPS sintered composite materials against volume fraction of GNP and GNT (vol. %) as compared to the monolithic FeCo alloy.

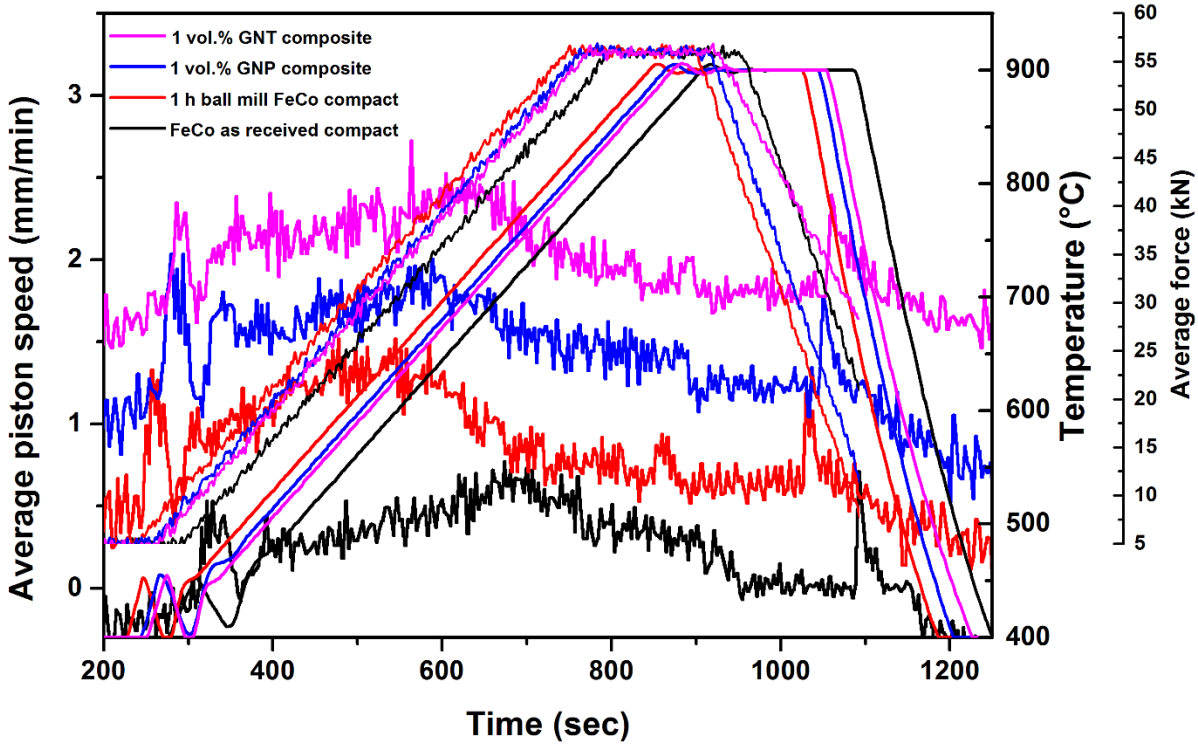

Fig.5. Change of temperature, average force and piston speed against time for the indicated materials during SPS.

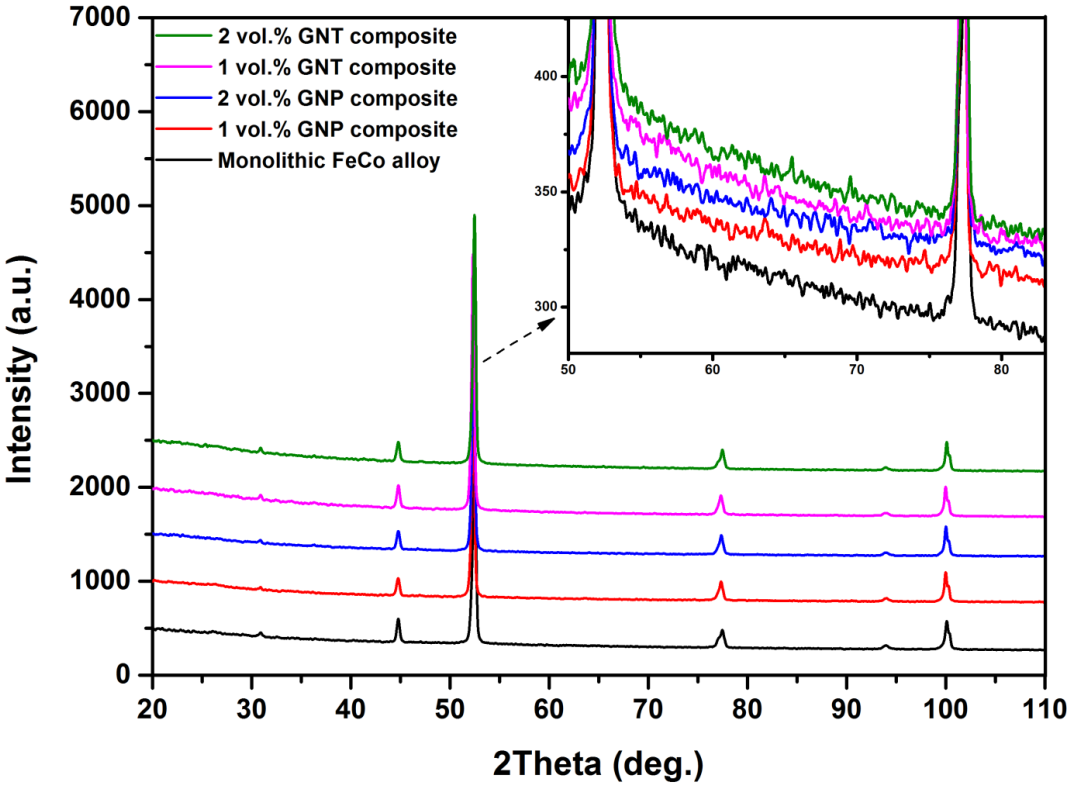

Fig.6. XRD patterns for FeCo as received; 1vol. % GNP composite; 2 vol.% GNP composite; 1 vol.% GNT and 2 vol.% GNT composite.

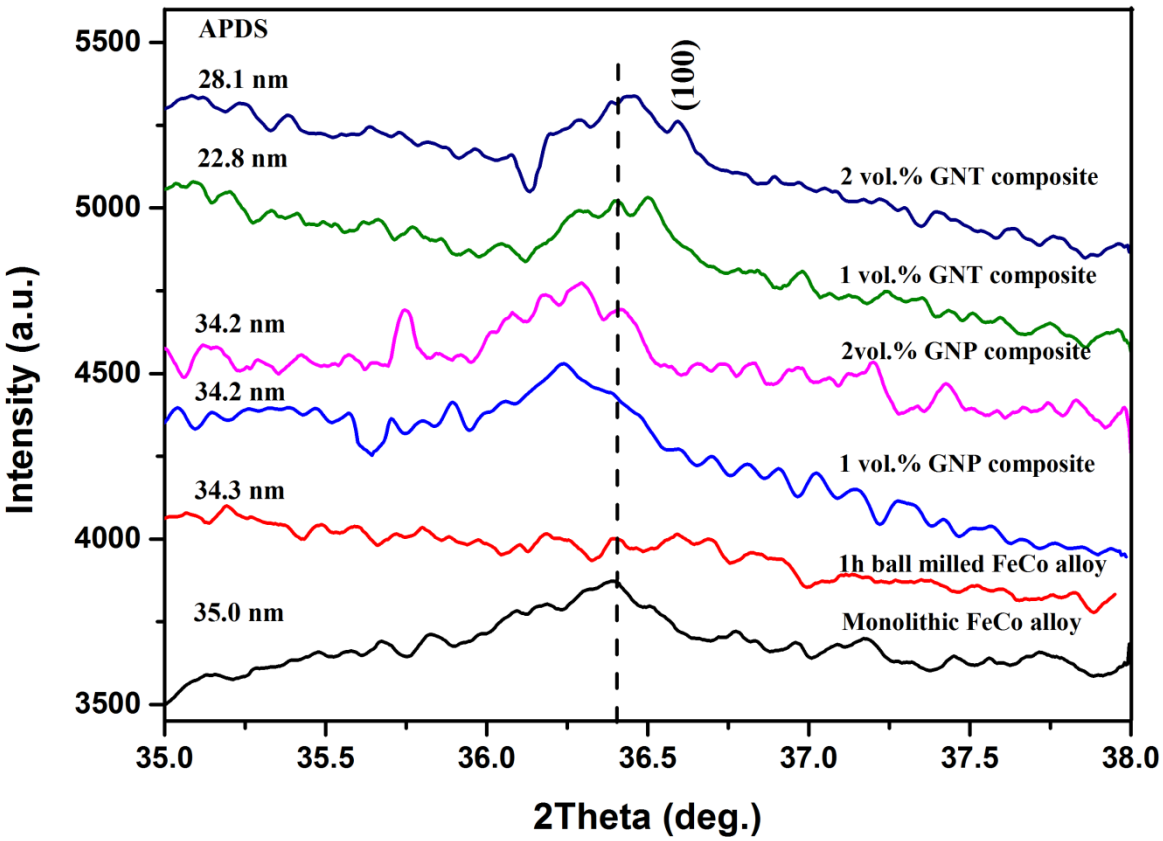

Fig.7. Slow scan XRD patterns show (100) super lattice line reflection with anti-phase domain size (APDS) of monolithic FeCo alloy, 1 h ball milled FeCo alloy and displayed composites.

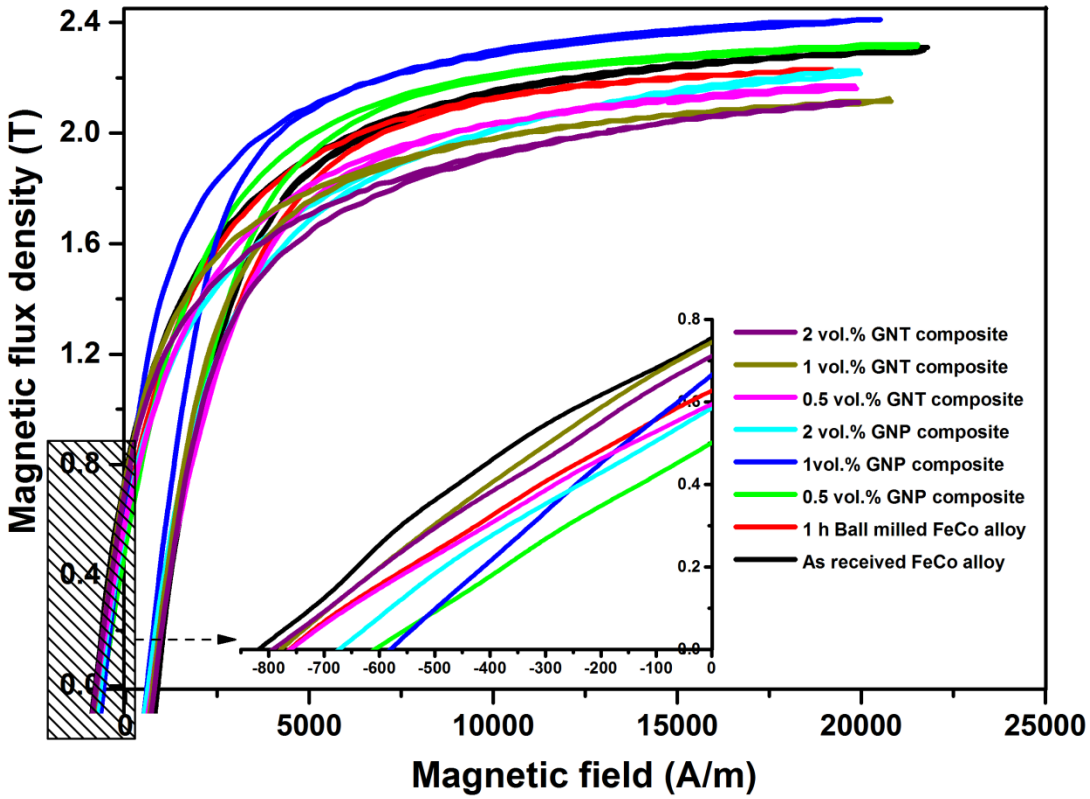

Fig.8. Upper half of the magnetic hysteresis curves of as a received FeCo alloy and composites for different volume fractions.

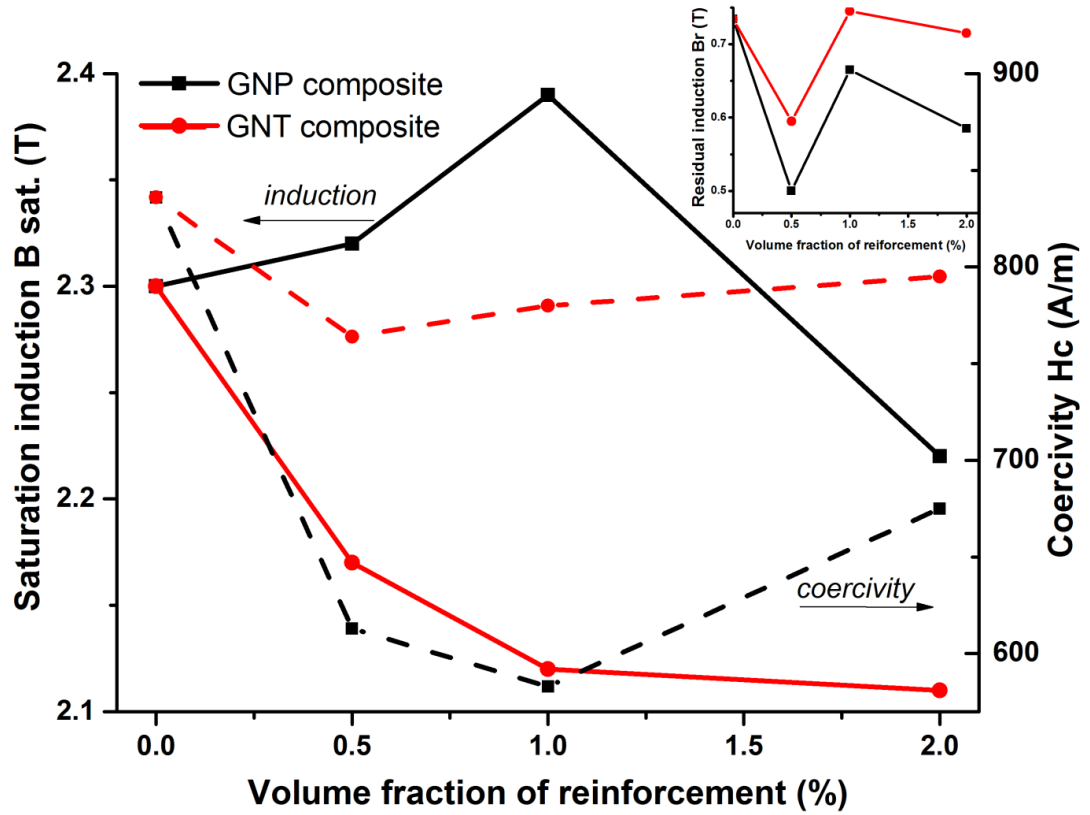

Fig.9. Effect of volume fraction of GNP and GNT on: saturation induction (solid lines); coercivity (dashed lines) and remanence (insert) of (Fe50Co) composites fabricated by spark

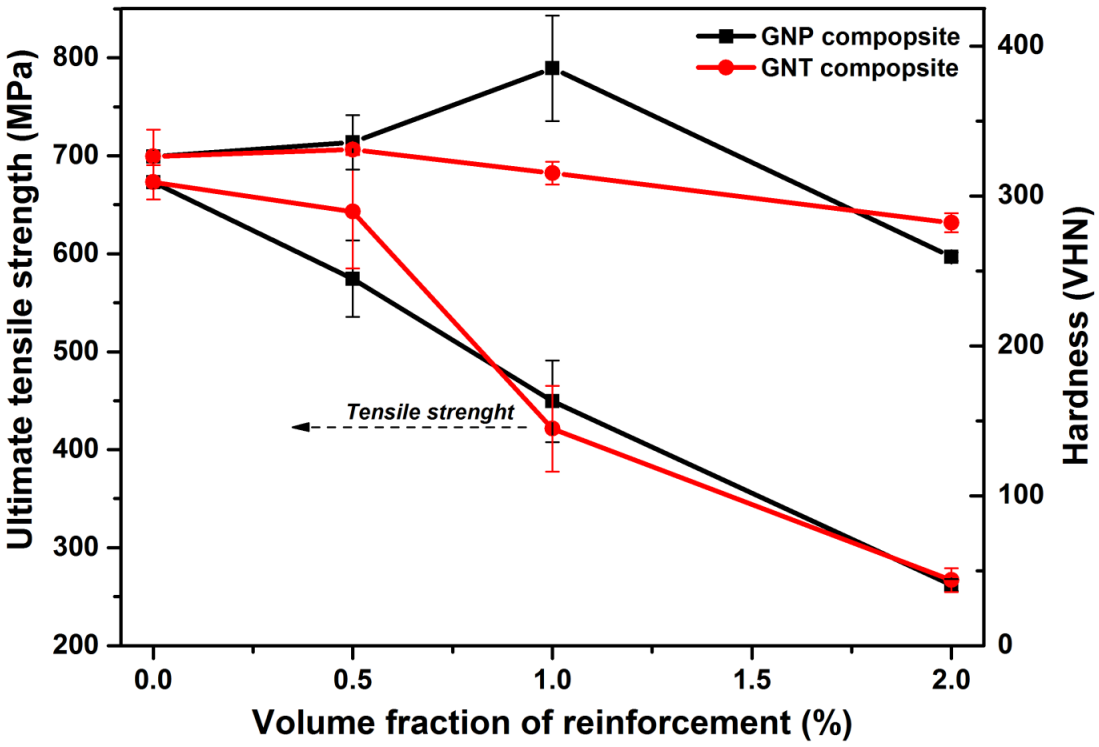

Fig.10. Effect of volume fraction of GNP and GNT on: tensile strength and hardness of Fe50Co composites fabricated by spark plasma sintering.

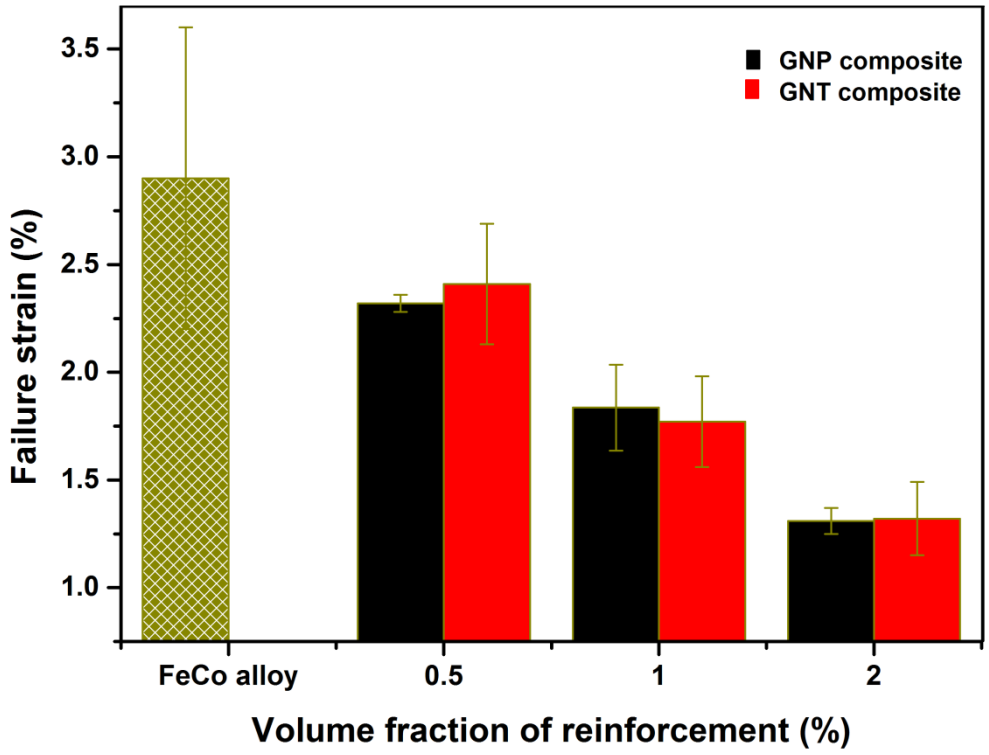

Fig.11. Effect of volume fraction of GNP and GNT on failure strain of Fe50Co composites fabricated by spark plasma sintering.

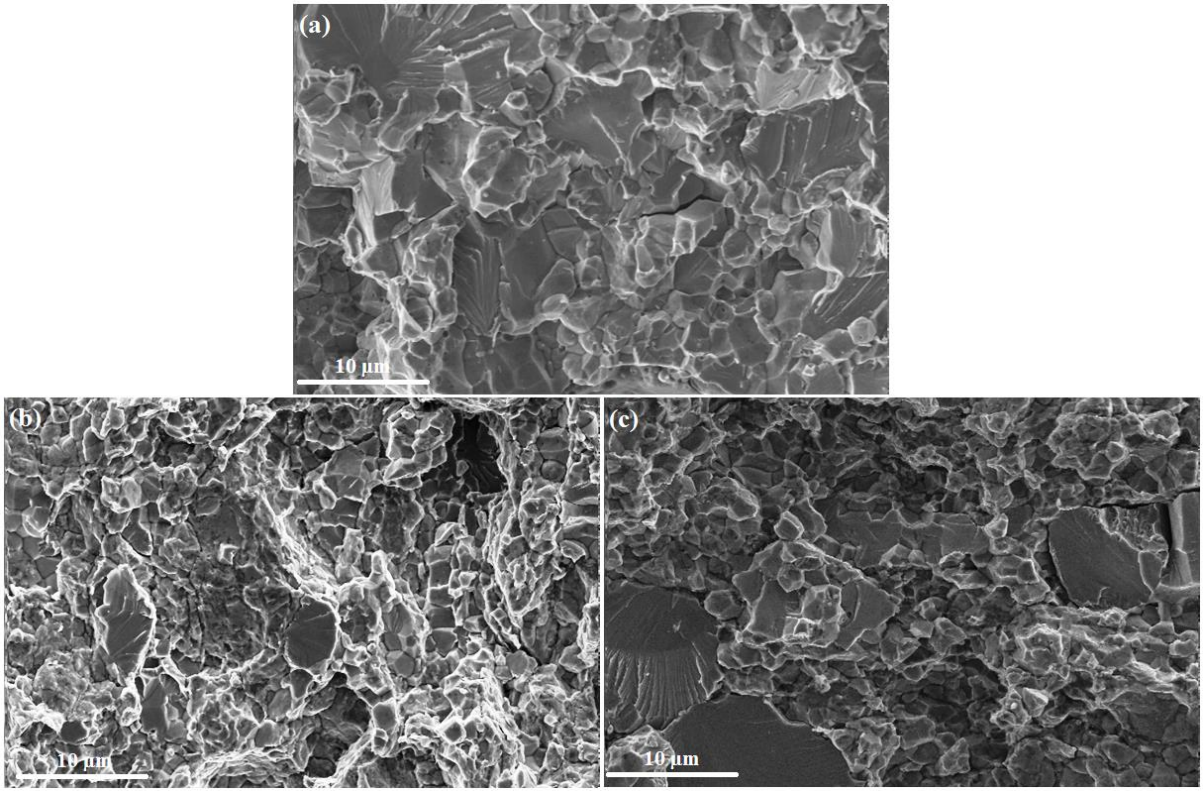

Fig.12. Fractographic images of: (a) as received FeCo alloy; (b) 1 vol. % GNP composites; and (c) 1 vol. % GNT composites fabricated by spark plasma sintering.

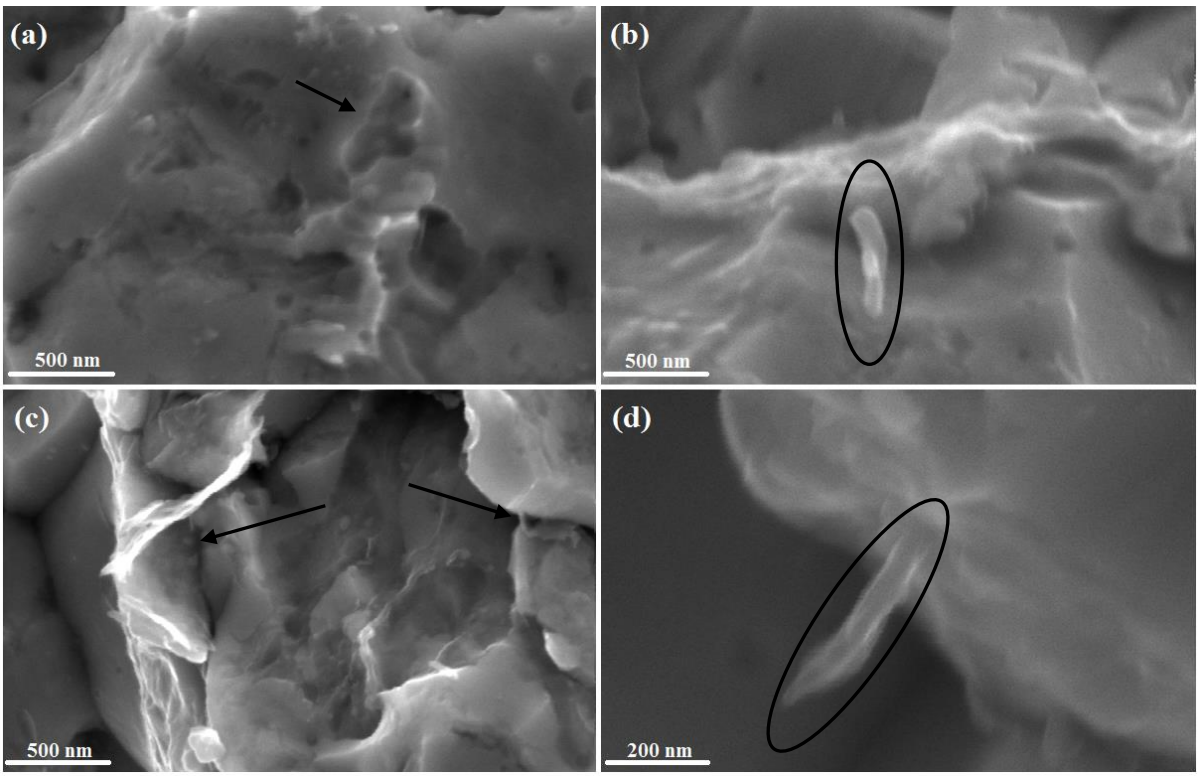

Fig.13. High magnification of fractographic images; (a, c) 0.5 and 1 vol. % GNP composites respectively; (b, d) 0.5 and 1 vol. % GNT composites respectively. The arrows show pull-out of GNP (a), thin and overlapped GNP(c). Ellipses exhibit CNTs bridging (b) and pull-out from GNPs (d).

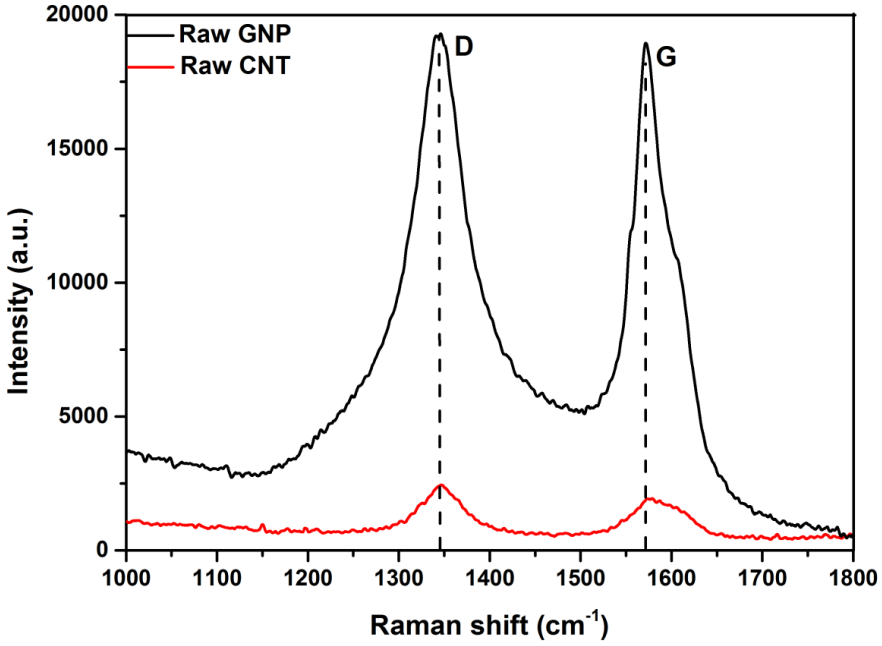

Fig.14. Raman spectra of Carbon nanotube and Graphene nanoplatelet.

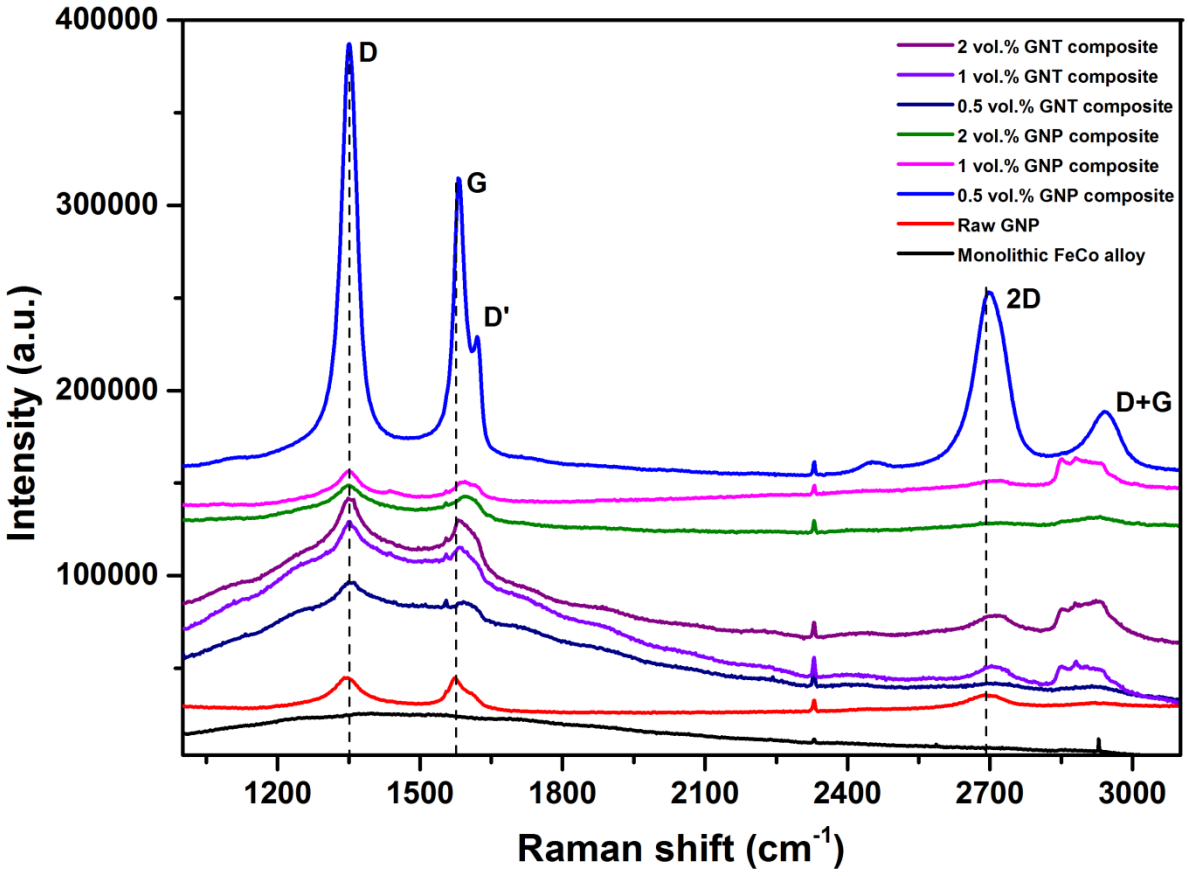

Fig.15. Raman spectra of GNP, GNT composites and as-received graphene.

Table 1: Raman data of sintered materials.

State	$R=I_D/I_G$	ω_G (cm^{-1})	ω_{2D} (cm^{-1})
Raw GNP	1.00	1573.0	2691.0
Raw CNT	1.11	1578.0	2691.0
0.5 vol.% GNP composite	1.37	1581.6	2699.8
1 vol.% GNP composite	1.15	1595.0	2708.6
2 vol.% GNP composite	1.09	1595.8	2716.4
0.5 vol.% GNT composite	1.07	1586.6	2710.7
1 vol.% GNT composite	1.06	1583.2	2703.5
2 vol.% GNT composite	1.06	1585.5	2709.0